PAPER

Check for updates

Use of surface-modified porous silicon nanoparticles to deliver temozolomide with enhanced pharmacokinetic and therapeutic efficacy for intracranial glioblastoma in mice†

Seulgi Shin,[abc] Hyejung Jo,[a] Tomoyo Agura,[a] Seoyoun Jeong,[a] Hyovin Ahn,[a] Yejin Kim*[ab] and Jae Seung Kang ![ORCID] *[abd]

Glioblastoma (GBM) is one of the most common and fatal primary brain tumors, with a 5-year survival rate of 7.2%. The standard treatment for GBM involves surgical resection followed by chemoradiotherapy, and temozolomide (TMZ) is currently the only approved chemotherapeutic agent for the treatment of GBM. However, hydrolytic instability and insufficient drug accumulation are major challenges that limit the effectiveness of TMZ chemotherapy. To overcome these limitations, we have developed a drug delivery platform utilizing porous silicon nanoparticles (pSiNPs) to improve the stability and blood–brain barrier penetration of TMZ. The pSiNPs are synthesized *via* electrochemical etching and functionalized with octadecane. The octadecyl-modified pSiNP (pSiNP-C_{18}) demonstrates the superiority of loading efficiency, *in vivo* stability, and brain accumulation of TMZ. Treatment of intracranial tumor-bearing mice with TMZ-loaded pSiNP-C_{18} results in a decreased tumor burden and a corresponding increase in survival compared with equivalent free-drug dosing. Furthermore, the mice treated with TMZ-loaded nanoparticles do not exhibit *in vivo* toxicity, thus underscoring the preclinical potential of the pSiNP-based platform for the delivery of therapeutic agents to gliomas.

Introduction

Glioblastoma (GBM) is one of the most prevalent primary malignant brain tumors. Patients generally have a median survival rate of less than 1 year from diagnosis, and most patients die within 2 years, even under favorable conditions.[1–3] Although various therapeutic options, such as maximal surgery and concurrent chemoradiotherapy (CCRT), are presently accessible, their impact on extending patient survival remains limited.[4] Treatment limitations primarily arise from the rapid proliferation of tumor cells and challenges in delivering the drugs to the brain, given its restricted accessibility.[5]

[a] *Laboratory of Vitamin C and Antioxidant Immunology, Department of Anatomy and Cell Biology, Seoul National University College of Medicine, Seoul 03080, Republic of Korea. E-mail: bbambaya921@snu.ac.kr, genius29@snu.ac.kr*

[b] *Institute of Allergy and Clinical Immunology, Seoul National University Medical Research Center, Seoul 03080, Republic of Korea*

[c] *Department of Research and Development, N therapeutics Co., Ltd, Seoul 08813, Republic of Korea*

[d] *Department of Applied Bioengineering, Graduate School of Convergence Science and Technology, Seoul National University, Seoul 08826, Republic of Korea*

† Electronic supplementary information (ESI) available. See DOI: https://doi.org/10.1039/d4tb00631c

Temozolomide (TMZ) is a primary chemotherapy agent that is currently utilized in clinical practice for GBM treatment, and it is administered in combination with radiotherapy.[6] TMZ has a small molecular weight (194.15 g mol^{-1}) and lipophilicity (log P 1.4), which enables it to be taken orally and pass through the blood–brain barrier.[7,8] TMZ spontaneously hydrolyzes under physiological conditions to form its active metabolite, 3-methyl-(triazen-1-yl)imidazole-4-carboxamide (MTIC). MTIC breaks down into 5-amino-imidazole-4-carboxamide (AIC) and methyl diazonium cation (MC). MC alkylates genomic DNA at the N7 and O6 sites of guanine and the N3 position of adenine, which induces a nucleotide mismatch, replacing cytosine with thymine during subsequent replication cycles.[9] The mismatch error of DNA replication ultimately leads to tumor cell death.[10] However, it has certain limitations, including a relatively short half-life of approximately 1.8 h and rapid *in vivo* clearance, resulting in restricted tumor uptake, typically ranging from 10–20%.[11,12] This results in frequent dosing to maintain the anti-tumor efficacy of TMZ, which can have side effects such as thrombocytopenia, nausea, and vomiting.[13] Furthermore, because of poor accumulation of TMZ in tumors, the peripheral and core glioblastoma cells are exposed to different concentrations of TMZ, which results in heterogeneous responses and resistance to TMZ.[14] Although increasing the dose of TMZ is

This journal is © The Royal Society of Chemistry 2024

J. Mater. Chem. B, 2024, **12**, 9335–9344 | 9335

expected to overcome these limitations, TMZ has a limited therapeutic index with significant dose-limiting side effects, such as myelosuppression and cardiomyopathy.[15,16] Considering that these limitations originate from the poor delivery of TMZ to the tumor site, there is a need to develop a method to deliver TMZ to the tumor more efficiently with fewer side effects.

Nanostructured materials have emerged as promising candidates for drug delivery, particularly in the context of cancer treatment.[17] Within the biomedical field, types of nanomaterials have been introduced and gained considerable attention due to their demonstrated potential in overcoming the significant limitations of pharmacologically active agents, including poor water solubility, low biological stability, and inefficacy in achieving *in vivo* targeting.[18–20] Among numerous nanoparticles developed, porous silicon nanoparticles (pSiNPs) have garnered considerable interest as a promising platform for drug delivery systems because of their remarkable characteristics. pSiNPs are made from silicon wafers *via* an electrochemical etching process.[21] The electrochemical etching process allows pSiNPs to have a porous structure with a high surface area.[22] It enables the pSiNPs to accommodate diverse therapeutic agents, including chemical drugs, nucleic acids, and peptides/proteins.[23–26] pSiNPs are also biodegradable under physiological conditions *via* oxidative hydrolysis in aqueous solutions.[27] The resulting degradation byproduct, silicic acid $(Si(OH)_4)$, is non-toxic and excreted by the urine.[28,29] In addition, the surface of pSiNPs can be functionalized by binding a variety of reagents through diverse chemical reactions for various purposes, such as high loading efficiency, enhanced stability, controlled drug release, or target disease specificity.[30,31]

In this study, we developed octadecane-modified pSiNPs to deliver TMZ for the treatment of intracranial GBM tumors. We demonstrate the increased concentration of delivered TMZ using octadecane-modified particles in the brain tissue of mice. Furthermore, we reveal that tumor-bearing mice treated with TMZ-loaded pSiNPs have decreased tumor burden compared with mice treated with free TMZ. It demonstrates the potential application of this silicon nanoparticle-based platform to improve outcomes for patients with GBM.

Materials and methods

Preparation of pSiNPs

The pSiNPs were prepared by electrochemical etching of boron-doped p-type silicon wafers in an electrolyte solution consisting of 48% hydrofluoric acid (HF, Millipore, MA, USA) and 99.5% ethanol (Millipore) in a ratio of 3 : 1 (v/v). The etching process was conducted using a platinum wire as a counter electrode in an etch cell made of PTFE (Redox me, Sweden). Prior to etching, the wafer surface was anodized electrochemically by applying a 200 mA $(cm^2)^{-1}$ current for 30 s in HF electrolyte solution and cleaned using 1 M of potassium hydroxide solution (KOH, Sigma, MO, USA). The etching of the silicon wafer was performed using a specific waveform consisting of a high current of 50 mA $(cm^2)^{-1}$ for 1.2 s, followed by a low current of 400 mA $(cm^2)^{-1}$ for 0.363 s, and

repeated for 500 cycles with a power supply (2460 source meter, Keithly, OH, USA). This process resulted in the formation of a thin porous silicon film on the wafer surface. The thin film was detached from the wafer by applying a current of 34.4 mA $(cm^2)^{-1}$ for 250 s in an electrolyte containing 48% HF and 99.5% ethanol in a ratio of 1 : 20 (v/v). The resulting free-standing film was then fractured into nanoparticles *via* ultrasonication (350 W) in an ethanol (4 mL) for 20 h. To remove aggregates, the fractured nanoparticles were then centrifuged at $2700 \times g$ for 3 min and the supernatant was collected. The collected supernatant was further centrifuged at $21\,000 \times g$ for 30 min to gather the pellet, removing particles that were too small. The resulting pSiNPs were stored in ethanol until use.

Preparation of pSiNP-C$_{18}$

The etched pSiNPs (3 mg) were dispersed in 1 mL of 95% octadecene solution (Sigma, MO, USA) and irritated in a microwave (700 W) for 5 min. To remove excess octadecene, the pSiNPs were washed three times with ethanol. The resulting pSiNPs were referred to as pSiNP-C$_{18}$. In all procedures, washing was performed by centrifugation at $21\,000 \times g$ for 30 min and resuspension was performed by ultrasonication.

Preparation of TMZ loaded pSiNPs

To load TMZ (Sigma) onto the pSiNPs, 1 mg of pSiNP and pSiNP-C18 were dispersed in a solution of 900 μL of ethanol and 100 μL TMZ (2 mg, 0.01 mmol in dimethly sulfoxide [DMSO]) was added dropwise at 4 °C. The solution was then transferred into a 4-mL glass vial containing a magnetic bar. The loading was performed on a 600-RPM magnetic stirrer at 4 °C for 24 h. The resulting pSiNP-H[TMZ] and pSiNP-C$_{18}$[TMZ] were then washed three times with ethanol and stored at 4 °C before use. To measure the loading efficiency, the supernatants from every washing procedure were collected and analyzed.

The loading efficiency of TMZ was determined using HPLC (Thermo Fisher Scientific, MA, USA) system consisting of a Dionex Ultimate 3000 series RS pump (LPG-3400SD), a Dionex Ultimate 3000 series Diode Array Detector (DAD-3000), a Dionex Ultimate 3000 series column department (TCC-3000SD) and a Dionex Ultimate 3000 series autosampler (WPS-3000TSL) controlled by Chromeleon 7.2.9 software. HPLC analysis was performed using a Thermo Hypersil GOLD aQ C18 column (150 mm × 4.6 mm × 5 μm, Thermo Fisher Scientific) as the stationary phase and mobile phase consisting of HPLC-grade water (J. T. Baker, PA, USA) containing 0.5% acetic acid and methanol (J. T. Baker) mixture in a ratio of 10 : 90 (v/v). The flow rate was 1 mL min^{-1} and the detection wavelength was 330 nm. The loading efficiency was calculated according to eqn (1) as follows:

$$\text{Loading efficiency} \ (\%) = \frac{(\text{Loaded drug mass})}{(\text{Total mass of loaded pSiNPs})} \times 100$$

$$(1)$$

9336 | *J. Mater. Chem. B*, 2024, **12**, 9335–9344

This journal is © The Royal Society of Chemistry 2024

Characterization of pSiNPs

A Malvern Zetasizer Pro (Malvern Panalytical, UK) was used to determine the hydrodynamic size and ζ-potential of the pSiNPs. A NICOLEY iS5 series FTIR sprectrometer (Thermo Fisher Scientific) fitted with an iD7 ATR accessory (Thermo Fisher Scientific) was used to evaluate the surface chemistry of pSiNPs through FTIR spectra. A JEM-1400 electron microscope (JEOL, Tokyo, Japan) fitted with a carbon film grid (Electron Microscopy Sciences, PA, USA) was used to obtain the pSiNPs TEM images.

Measurement of TMZ release profiles from pSiNPs

To measure the in vitro release profiles of TMZ from pSiNPs, 1 mg of pSiNP-H[TMZ] and pSiNP-C18[TMZ] were dispersed in PBS (pH7.2) for 6 h at 37 °C. Supernatants were collected at 0.5, 1, 3, and 6 h and stored at 4 °C until analysis. The percentage of released TMZ was calculated by the cumulative release across the time points. The released TMZ in the supernatants was analyzed by HPLC.

Cell culture

The human GBM cell line U87MG was purchased from ATCC. U87MG was maintained in Dulbecco's modified Eagle's medium (Welgene, Gyeongsangbuk-do, Korea) containing 10% fetal bovine serum (Gibco, CA, USA), 100 UI mL^{-1} penicillin/streptomycin (Welgene) at 37 °C in a humidified atmosphere with 5% CO_2.

Animals

Immunodeficient BALB/c nude mice were purchased from OrientBio (Gyeonggi-do, Korea), and ICR mice were purchased from KOATECH (Gyeonggi-do, Korea). The mice were housed on a 12/12 h light/dark cycle in pathogen-free facilities at the Seoul National University College of Medicine. All experiments were reviewed and approved by the Institutional Animal Care and Use Committee of Seoul National University (IACUC No. SNU-230511-9, SNU-230607-2).

Generation of an orthotopic GBM mouse model

To generate an orthotopic GBM mouse model, BALB/c nude mice (male, 8 weeks-old) were anesthetized with a 200 μL mixture of Zoletil 50 (Virbac, France), Rompun (Elanco, IN, USA), and PBS mixture (1 : 1 : 4 v/v) and placed in a stereotaxic instrument (KOPF instruments, LA, USA). The mice were then administered an injection of 1×10^6 U87MG cells suspended in PBS at the following coordinates: anteroposterior: 1.7 mm, mediolateral: 0.5 mm, and dorsoventral: −3.2 mm from the skull bregma. The mice were weighed 2–3 times a week, and at 12 days post xenograft surgery, the mice were randomly assigned to 6 groups ($n = 10$): control (normal saline), TMZ (3 mg kg^{-1}), pSiNP-H, pSiNP-C$_{18}$, pSiNP-H[TMZ], and pSiNP-C$_{18}$[TMZ]. The drug then was intravenously (i.v.) injected via the tail vein of mice every other day and received a total of five injections. After the injection course was completed, the tumor size was measured by MRI. On day 22, mice ($n = 4$ per group)

were perfused and organs were fixed with 4% paraformaldehyde. The fixed tissues were dehydrated and embedded in paraffin. Blood samples were also collected and centrifuged at $600 \times g$ for 10 min at 4 °C. The resulting serum was stored at −80 °C until use.

Immunohistochemistry

The paraffin-embedded tissue blocks were sectioned into 4-μm thick slices. After deparaffinization and hydration, the antigen epitopes were retrieved by heating with 0.1 M citrate buffer (pH 6.0) in a microwave. Subsequently, the endogenous peroxidase was blocked with H_2O_2, and non-specific signals were blocked by incubating the sections with blocking solution (Vector Laboratories, Burlingame, CA, USA) containing 5% goat serum for 1 h at room temperature. To examine the expression levels of Ki67 and cleaved caspase-3, the tissue sections were incubated overnight with anti-Ki67 (1 : 150; Abcam, Cambridge, UK) and anti-cleaved caspase-3 (1 : 150; Cell Signaling Technology, MA, USA) anti-bodies in a humidified chamber at 4 °C. The sections were subsequently incubated with biotinylated goat anti-rat immunoglobulin (1 : 250; Vector Laboratories) for 1 h at room temperature. ABC solution (Vector Laboratories) was loaded onto the sections for 30 min and a DAB kit (Vector Laboratories) was used for chromogenic detection. After counterstaining with hematoxylin, dehydration, and clearing, the tissue sections were mounted onto glass slides (Life Technologies, Frederick, MD, USA). An Olympus AX-70 microscope equipped with a motorized stage (Olympus, Melville, NY, USA) was used for visualization and data were analyzed using MCID 6.0 Elite Imaging Software (GE Healthcare, Piscataway, NJ, USA).

MRI imaging

An MRI was performed to measure the tumor volume. Mice were anesthetized with 2% isoflurane and secured in an MR SOLUTION 3-T instrument (MR Solutions, CO, USA). A fast-spin echo sequence was employed and, T2-weighted images (repetition time (TR)/echo time (TE): 3000/68 ms, field of view: 28 × 28 mm, matrix: 256 × 256, slice thickness = 0.8 mm) were used to localize the tumor. Tumor volumes were calculated using a Radiant DICOM viewer (Medixant, Poznan, Poland). Tumor volume was calculated using eqn (2) as follows:

$$\text{Tumor volume } (\text{mm}^3) = \frac{\pi}{2} \times \text{width} \times \text{height}^2 \qquad (2)$$

Plasma biochemical assay

To evaluate the toxicity of pSiNPs on liver and kidney function, the ALT, AST, and creatinine levels were determined in the mouse plasma. The plasma was analyzed using an Alanine Transaminase Activity Assay Kit (Abcam), ALT, and AST Activity Assay kit (Abcam), Aspartate Aminotransferase Activity Assay Kit (Abcam), and Creatinine Assay Kit (Abcam) in accordance with the manufacturer's instructions.

This journal is © The Royal Society of Chemistry 2024

J. Mater. Chem. B, 2024, 12, 9335–9344 | 9337

Pharmacokinetics of TMZ-loaded on pSiNP in mice

To investigate the pharmacokinetics of TMZ-loaded on pSiNP, TMZ, pSiNP-H[TMZ], and pSiNP-C$_{18}$[TMZ] were intravenously injected *via* the tail vein into ICR mice (male, 8 weeks old) at a dose of 20 mg kg^{-1}. At 0.5, 1, and 4 h after post-drug administration, the mice were anesthetized and perfused with saline. The blood was centrifuged at 14 000×g at 4 °C for 15 min, and the serum was collected. A total of 100 μL of serum was mixed with 100 μL of 1% acetic acid in distilled water and analyzed by HPLC. After the mice were perfused, their brains were harvested and weighed. The brains were then homogenized in 1 mL of saline, and the homogenates were centrifuged at 14 000×g at 4 °C for 15 min. The supernatants were mixed with 1% acetic acid in distilled water and centrifuged at 14 000×g at 4 °C for 15 min. The resulting supernatants were then analyzed by HPLC.

Statistical analysis

Data are presented as the mean ± standard deviation (SD), except for the data of animal expression data, which are presented as the mean ± standard error of the mean (SEM).

A two-tailed *t*-test was performed when two groups were compared. One-way or two-way analysis of variance (ANOVA) was performed when multiple groups were compared, depending on the number of independent variables. Statistical analysis was performed using the Prism software (GraphPad Software, Inc., CA, USA).

Results and discussion

Preparation and surface modification of pSiNPs for TMZ loading

The process of pSiNPs synthesis is presented in Fig. 1. Nanoparticles were produced using the electrochemical etching method. A p-type silicon wafer was used as the raw material, and a mixture of hydrofluoric acid (HF) and ethanol served as the etchant (Fig. 1A). The porous silicon film was constructed on the wafer by applying a square-wave pulse current and lifted off by a constant current. Ultrasonication and centrifugation were then performed to produce nanoparticles with hydrogen-terminated surfaces named pSiNP-H (Fig. 1B). To obtain a functional and stable interface, the reactive Si–H surface was
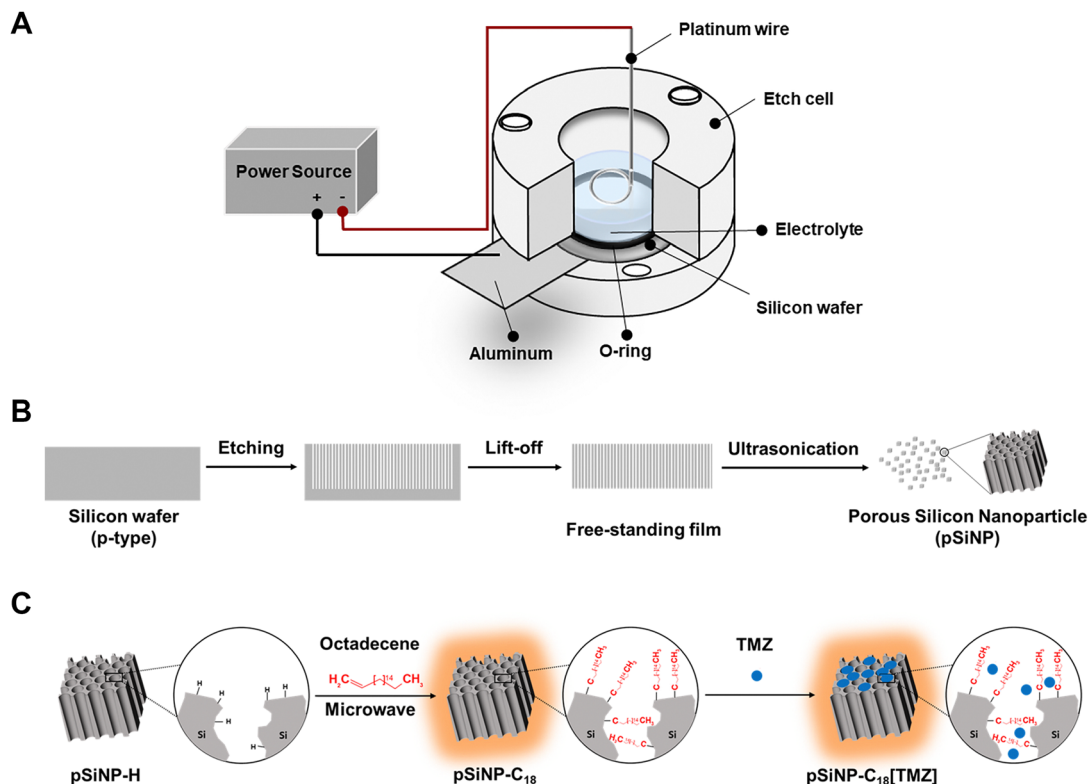

Fig. 1 Preparation and surface modification of porous silicon nanoparticles (pSiNPs) for temozolomide (TMZ) loading. (A) Schematic of etching cell with a platinum wire for cathode and silicon wafer for anode. The electrolyte used was a mixture of 48% hydrofluoric acid and 99.5% ethanol in a volume ratio of 3 : 1 (v/v). (B) Process of preparing pSiNPs *via* etching and ultrasonication. The silicon wafer was etched using a waveform comprising a high current of 50 mA (cm^2)$^{-1}$ for 1.2 s, followed by a low current of 400 mA (cm^2)$^{-1}$ for 0.363 s, repeated for 500 cycles with a power supply. This process resulted in a thin porous silicon film on the wafer surface, which was lifted off using a current of 34.4 mA (cm^2)$^{-1}$ for 250 s in an electrolyte containing 1 : 20 (v/v) 48% HF and 99.5% ethanol. The resulting free-standing film was fractured into nanoparticles *via* ultrasonication in ethanol for 20 h. (C) Schematic of pSiNP surface modification and TMZ loading. For surface modification, 3 mg of pSiNPs were dispersed in 1 mL of octadecene, and microwave irradiation was used to induce binding. For TMZ loading, 1 mg of pSiNPs were incubated with 2 mg of TMZ in ethanol at 4 °C for 24 h.

9338 | *J. Mater. Chem. B*, 2024, **12**, 9335–9344

This journal is © The Royal Society of Chemistry 2024

modified with octadecane. To introduce the hydrocarbon chain, a hydrosilylation reaction with an unsaturated carbon chain, 1-octadecene, was achieved using microwave energy. The modified particles were, therefore, named pSiNP-C_{18} throughout this study. TMZ was introduced into the pores and surfaces of each nanoparticle, pSiNP-H or pSiNP-C_{18}, through hydrophobic interactions (Fig. 1C).

Characterization of surface-modified pSiNPs loaded with TMZ

The carbonization of the particle surface was monitored by Fourier transform infrared (FTIR) spectroscopy (Fig. 2A). The spectrum of pSiNP-H (blue line) displays the Si–H peak stretching at 2110 cm^{-1}. In the case of pSiNP-C_{18} (red line), modified with octadecane, displays additional strong peaks at 2850 and 2950 cm^{-1} associated with C–H stretching. This data indicates
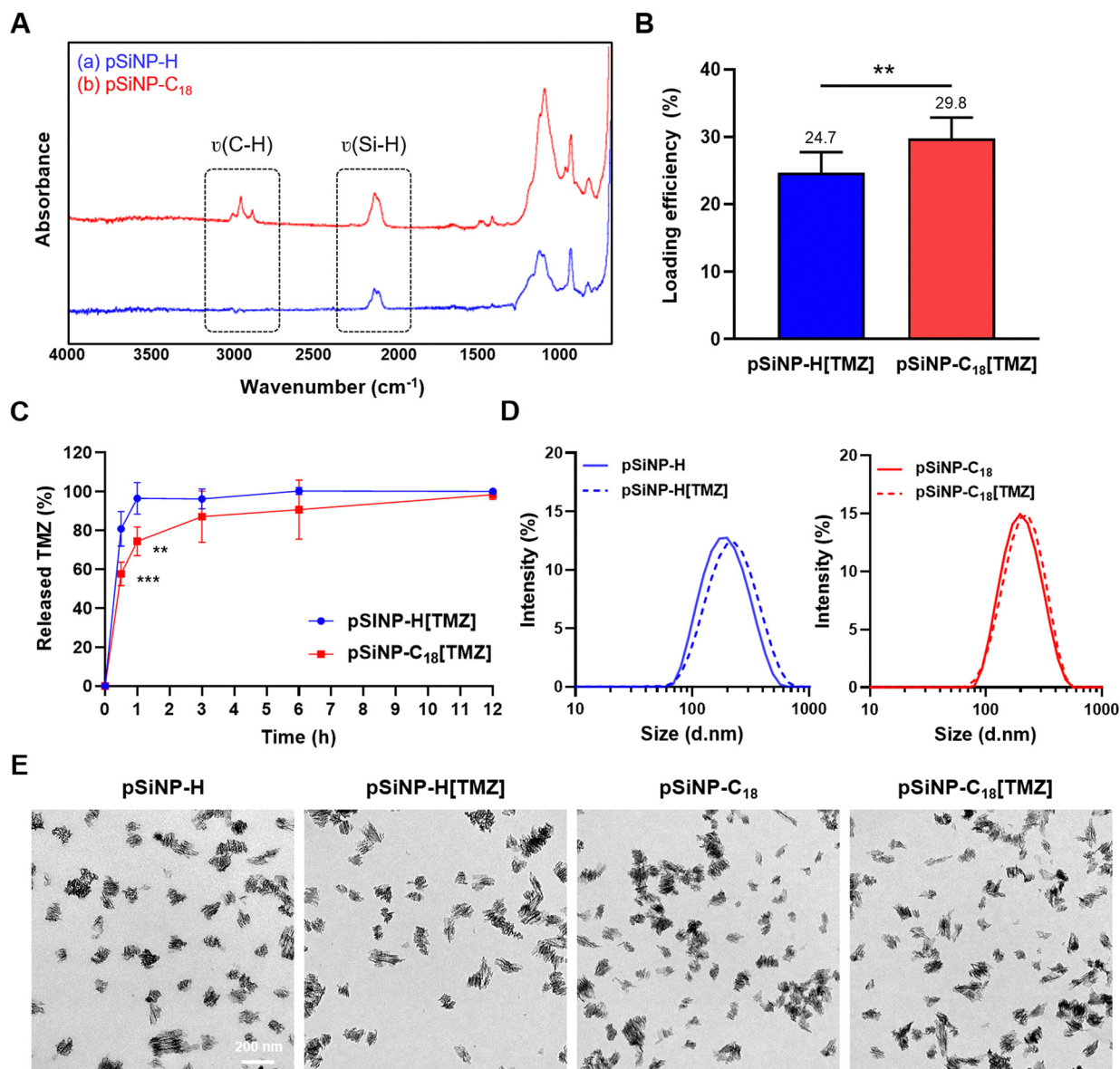

Fig. 2 Characterization of surfaced-modified porous silicon nanoparticles (pSiNPs) loaded with temozolomide (TMZ). (A) Attenuated total reflectance Fourier transform infrared (ATR-FTIR) spectra of pSiNPs before and after surface modification. Symbol: v = streching. The pSiNP-H displayed bands associated with the Si–H functionality, a band for v(Si–H) at 2110 cm^{-1}. The pSiNP-C_{18} showed an additional strong band at 2850–2950 cm^{-1} associated with v(C–H). (B) Loading efficiency of pSiNP-H[TMZ] and pSiNP-C_{18}[TMZ]. Loaded TMZ was calculated by subtracting the amount of unloaded drug from the total drug input after incubating TMZ with the pSiNPs for 24 h. The data are presented as the mean ± standard deviation (SD) of three independent experiments. A two-tailed t-test was performed. ***$p < 0.001$ (C) TMZ release profiles of pSiNP-H or pSiNP-C_{18}. The release profiles depict percentage of TMZ released from the nanoparticles into the phosphate-buffered saline over time at 37 °C. The data are presented as the mean ± standard deviation (SD) of four independent experiments. A two-tailed t-test was performed. **$p < 0.01$,***$p < 0.001$. (D) Intensity distribution of the hydrodynamic diameter of pSiNPs was measured by dynamic light scattering. (E) Representative transmission electron microscopy (TEM) images of pSiNPs before and after surface modification and TMZ loading. Scale bar = 200 nm.

This journal is © The Royal Society of Chemistry 2024

J. Mater. Chem. B, 2024, **12**, 9335–9344 | **9339**

that octadecane was successfully grafted onto the surface of the pSiNPs. Surface modification of the pSiNP affected the drug loading efficiency. After incubation of TMZ with the nanoparticles in ethanol for 24 h, TMZ was loaded onto intact pSiNPs with an efficiency of 24.1% and on the surface-modified pSiNPs with a greater efficiency of 29.8% (Fig. 2B). This result implies an increase in the hydrophobic interaction between TMZ and carbon chains on the surface of the pSiNPs. The drug release profiles for both the TMZ-loaded nanoparticles were measured over time when the nanoparticles were dissolved in a phosphate-buffered saline (PBS) solution at 37 °C. Samples were collected at multiple time points over 12 h and analyzed using high-performance liquid chromatography (HPLC) to measure the drug release from the nanoparticles. For pSiNP-H loaded with TMZ (pSiNP-H[TMZ]), the drug was almost completely released within 1 h, showing release rates of $80.0 \pm 8.9\%$ and $96.5 \pm 8.1\%$ at 0.5 h and 1 h, respectively. In contrast, pSiNP-C_{18} loaded with TMZ (pSiNP-C_{18}[TMZ]) exhibited a more gradual release profile of $57.6 \pm 6.1\%$, $74.5 \pm 7.5\%$, and $87.1 \pm 13.3\%$ at 0.5 h, 1 h, and 3 h, respectively (Fig. 2C). This result indicates the slower dissolution of the octadecyl-modified nanoparticles in PBS, which contributes to the enhanced stability of TMZ.

The physical properties of the pSiNPs were further measured using dynamic light scattering (DLS). Before drug loading, pSiNP-H and pSiNP-C_{18} displayed an average hydrodynamic diameter of 191.6 ± 0.9 nm (polydispersity index (PDI): 0.25 ± 0.02) and 206.3 ± 2.2 nm (PDI: 0.25 ± 0.03) and a ζ-potential of -26.6 ± 3.08 mV and -28.9 ± 1.87 mV, respectively. The TMZ-loaded particles, pSiNP-H[TMZ] and pSiNP-C_{18}[TMZ], exhibited average sizes of 195.9 ± 15.5 nm (PDI: 0.13 ± 0.01) and 211.6 ± 12.8 nm (PDI: 0.12 ± 0.03) and a ζ-potential of -28.4 ± 1.04 mV and -28.0 ± 2.71 mV, respectively (Table 1, Fig. 2D). The DLS data indicated that the surface modification with C18 slightly increased the size, whereas the drug loading with TMZ had minimal effect on the size, and no aggregates were observed. Drug loading and C18 conjugation did not significantly change the ζ-potential of the pSiNPs. The PDI values of all groups were between 0.1 and 0.3, which indicates that the pSiNPs had good uniformity. Transmission electron microscopy (TEM) images also showed a preserved pore structure and relatively homogeneous particle size (Fig. 2E). In conclusion, the size uniformity and overall appearance of the nanostructure were both successfully maintained after the C18 conjugation and drug loading processes.

To evaluate the cytotoxicity of TMZ-loaded nanoparticles, U87MG cells were treated with either 100 μM of TMZ or TMZ-loaded nanoparticles at an equivalent dose for 72 h, followed by cell cycle analysis via flow cytometry. As shown in Fig. S1 (ESI†), TMZ treatment resulted in cell cycle arrest in the G2/M phase, showing an approximately 2.5-fold increase compared to the control group. Similar effects were observed with pSiNP-H[TMZ] and pSiNP-C_{18}[TMZ] treatments. Both TMZ and TMZ-loaded pSiNPs also demonstrated a substantial increase in the sub-G1 population, indicative of apoptosis, relative to the control. These results indicate that TMZ-loaded pSiNPs maintain comparable anti-tumor efficacy to free TMZ in vitro, confirming that TMZ retains its physical and chemical properties throughout the loading process into pSiNPs.

Enhanced pharmacokinetics of TMZ-loaded pSiNPs

Given the potential of pSiNPs to enhance the in vivo stability of TMZ, we conducted a pharmacokinetic analysis of TMZ in mice. To assess the TMZ concentration in the blood and brain, 20 mg kg^{-1} doses of free TMZ, pSiNP-H[TMZ], and pSiNP-C_{18}[TMZ] were administered intravenously, followed by blood and brain tissue collection at various time points. The TMZ concentration was determined using HPLC in the plasma and brain lysates. In the plasma, the pSiNP-H[TMZ] injection group exhibited TMZ concentrations of 18.6 ± 2.3 μg mL^{-1} at 0.5 h and 18.1 ± 4.6 μg mL^{-1} at 1 h, which slightly surpassed those observed in the group that received free TMZ injection (16.7 ± 1.4 μg mL^{-1} at 0.5 h and 13.8 ± 2.2 μg mL^{-1} at 1 h). Conversely, the pSiNP-C_{18}[TMZ] injection group displayed the lowest TMZ concentration at 0.5 h (7.3 ± 3.7 μg mL^{-1}); however, at 1 h, it demonstrated a level approximately two times greater (29.0 ± 2.0 μg mL^{-1}) than that of the free TMZ injection group. TMZ was barely detectable in all groups after 4 h (Fig. 3A).

In the brain, pSiNP-H[TMZ] exhibited a TMZ concentration of 9.1 ± 0.9 μg g^{-1} at 0.5 h, which was similar to that of free TMZ (9.5 ± 1.0 μg g^{-1}). However, the pSiNP-H[TMZ] injection group maintained its brain TMZ concentration at 1 h, with a value of 8.8 ± 2.1 μg g^{-1}, while the free TMZ injection group experienced a rapid decline in TMZ levels (6.3 ± 1.5 μg g^{-1}). In the case of the pSiNP-C_{18}[TMZ] injection group, they exhibited the highest levels of brain TMZ concentration at 0.5 h (16.1 ± 1.5 μg g^{-1}) and 1 h (14.1 ± 2.3 μg g^{-1}) (Fig. 3B).

To evaluate brain-targeting efficiency, the brain-to-plasma concentration ratio at each time point was calculated. The

Table 1 Summary of of porous silicon nanoparticle size, zeta-potential, and polydispersity index. Average diameter, zeta-potential, and polydispersity indices of pSiNP-H, pSiNP-C_{18}, pSiNP-H[TMZ], and pSiNP-C_{18}[TMZ] were measured by dynamic light scattering

Nanoparticle	Z_{avg} $d_h{}^a$ [nm]	Zeta potential [mV]	Polydispersity index
pSiNP-H	191.6 ± 0.9	-26.62 ± 3.08	0.25 ± 0.02
pSiNP-C_{18}	206.3 ± 2.2	-28.93 ± 1.87	0.25 ± 0.03
pSiNP-H[TMZ]	195.9 ± 15.5	-28.44 ± 1.04	0.13 ± 0.01
pSiNP-C_{18}[TMZ]	211.6 ± 12.8	-27.96 ± 2.71	0.12 ± 0.03

^{a} Average diameters.

9340 | J. Mater. Chem. B, 2024, 12, 9335–9344

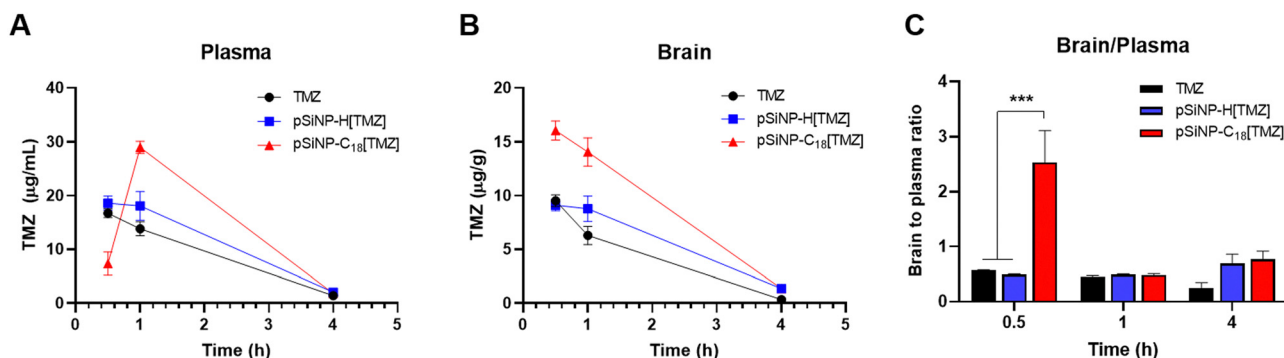This journal is © The Royal Society of Chemistry 2024

Fig. 3 Enhanced pharmacokinetics of temozolomide (TMZ)-loaded porous silicon nanoparticles (pSiNPs). (A) TMZ concentration in mouse plasma. The concentration of TMZ in mouse plasma was measured by HPLC following a single intravenous injection of 20 mg kg^{-1} free TMZ or an equivalent dose of TMZ-loaded pSiNPs in ICR mice (n = 3). (B) TMZ concentration in mouse brains. (C) The brain-to-plasma ratio for TMZ. The brain-to plasma concentration ratio at each time point was calculated as a ratio of brain concentration to plasma concentration. The data are presented as the mean ± standard error of the mean (SEM). A two-way ANOVA with Tukey's multiple comparisons test was performed. ***$p < 0.001$.

brain-to-plasma ratio of pSiNP-C$_{18}$[TMZ] was 2.53 ± 0.6 at 5 h, which was approximately five times greater than those of free TMZ and pSiNP-H[TMZ] (0.57 ± 0.01 and 0.49 ± 0.01, respectively). In addition, the brain-to-plasma ratio of pSiNP-C$_{18}$[TMZ] was highest at the initial time points, thus demonstrating that pSiNP-C$_{18}$[TMZ] rapidly permeates into the brain with no lag time (Fig. 3C).

Interestingly, the administration of pSiNP-C$_{18}$[TMZ] exhibits the lowest levels of TMZ in plasma and the highest levels in the brain at the initial time point. This is attributed to the sustained release profile of pSiNP-C$_{18}$, which effectively maintains the majority of TMZ encapsulated within the nanoparticles, thereby attenuating systemic exposure of free TMZ in the bloodstream. Furthermore, the enhanced brain permeation of pSiNP-C$_{18}$ is considered to underlie the heightened accumulation of TMZ in brain tissues. Conversely, pSiNP-H rapidly dissolves, releasing TMZ molecules quickly into the bloodstream, resulting in plasma TMZ concentrations comparable to those observed following the administration of free TMZ. This rapid-release kinetics leads to similar systemic exposure levels of TMZ at the initial time point. Collectively, these findings highlight the role of pSiNP-C$_{18}$ in protecting TMZ from rapid hydrolysis and enhancing brain uptake, thereby leading to increased accumulation in brain tissues compared to both pSiNP-H and free TMZ formulations.

Anti-tumor effect of TMZ-loaded pSiNPs in an orthotopic glioblastoma mouse model

To evaluate the *in vivo* anti-tumor effect of TMZ-loaded pSiNPs, U87MG cells were injected into the brain striatum of BALB/c nude mice. Twelve days after the injection, the mice received intravenous treatments with either 3 mg kg^{-1} of free TMZ or an equivalent dose of TMZ-loaded pSiNPs that were administered every other day for a total of five doses. After 22 days of tumorigenesis, intracranial tumors were visualized using magnetic resonance imaging (MRI) (Fig. 4A). The control and vehicle-treated groups (pSiNP-H and pSiNPC$_{18}$) displayed tumor volumes of 1.82 ± 0.11 mm^3, 1.80 ± 0.11 mm^3, and

1.66 ± 0.19 mm^3, respectively, whereas the TMZ-, pSiNP-H[TMZ]-, and pSiNP-C$_{18}$[TMZ]-treated group showed reduced tumor volumes of 1.17 ± 0.10 mm^3, 0.99 ± 0.05 mm^3, and 0.52 ± 0.06 mm^3, respectively (Fig. 4B and C). Compared with the control, the TMZ injection inhibited tumor growth by 35.7% ($p < 0.01$), whereas the pSiNP-H[TMZ] and pSiNP-C$_{18}$[TMZ] injections inhibited growth by 54.4% and 71.4% ($p < 0.001$), respectively. Additionally, when compared with the TMZ-treated mice, pSiNP-C$_{18}$[TMZ] treatment effectively reduced tumor growth by 55.6% ($p < 0.01$), whereas pSiNP-H[TMZ] treatment reduced the tumor growth by 15.4%, although this was not significant. Tumor tissues isolated from the mice's brains further confirmed the results observed in MRI images (Fig. S1, ESI†). Overall, our findings suggest that pSiNP-C$_{18}$[TMZ] is the most effective in inhibiting tumor growth in tumor-bearing mice.

Tumor cell proliferation was assessed by Ki67 immunostaining (Fig. 4D and E). Consistent with the tumor size results, the area of Ki67-positive cells decreased in the groups treated with TMZ, pSiNP-H[TMZ], and pSiNP-C$_{18}$[TMZ] compared with the control group. However, the most substantial decrease was observed in the pSiNP-C$_{18}$[TMZ]-treated group. Specifically, compared with the control, the Ki67-stained area in tumors decreased by 44.7%, 68.9%, and 76.1% in the TMZ-, pSiNP-H[TMZ]-, and pSiNP-C$_{18}$[TMZ]-treated groups, respectively ($p < 0.05$, $p < 0.001$, and $p < 0.0001$, respectively). Furthermore, the apoptosis levels in the tumor cells were assessed using cleaved caspase-3 immunostaining. As anticipated, treatment with pSiNP-C$_{18}$[TMZ] was the most effective at inducing tumor cell apoptosis, as evidenced by the highest expression level of cleaved caspase in the tumor cells. Specifically, the cleaved caspase-3-stained area in the tumors from the pSiNP-C$_{18}$[TMZ]-treated group was 4.14-fold greater than that of the control group. In comparison, the increases observed in the TMZ- and pSiNP-H[TMZ]-treated groups were 1.98- and 2.93-fold greater, respectively, compared to the control group.

To assess the survival rates, the remaining mice underwent two additional cycles of TMZ or TMZ-loaded pSiNPs therapy,
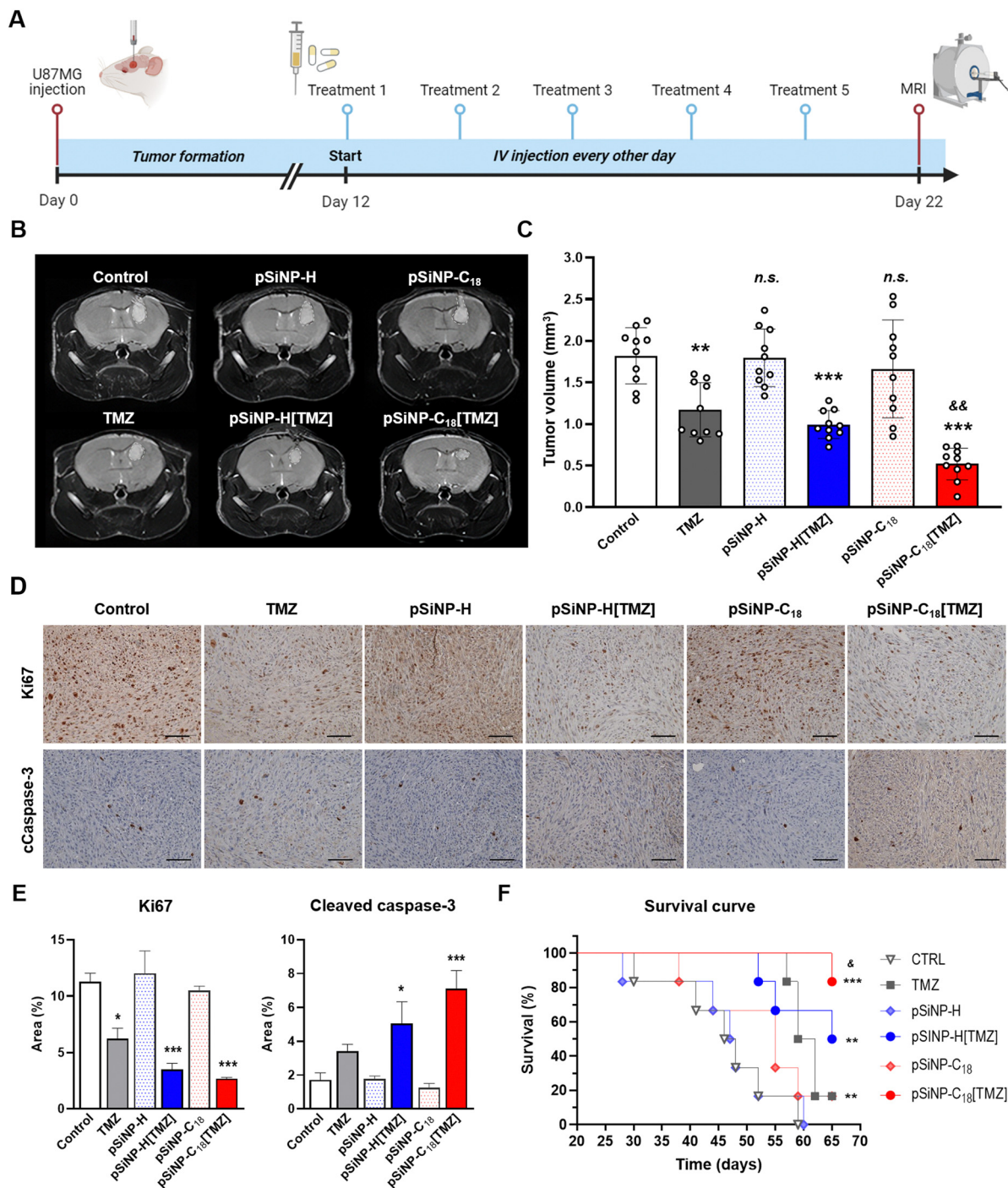
Fig. 4 Anti-tumor effect of temozolomide (TMZ)-loaded porous silicon nanoparticles (pSiNPs) in an orthotopic glioblastoma mouse model. (A) Schematic illustration of *in vivo* experimental schedule. U87MG cells were implanted into BALB/c nude mice *via* stereotactic injection of 1×10^6 cells per animal. Twelve days after glioblastoma cell injection, the mice received intravenous treatment with normal saline (control), TMZ (3 mg kg^{-1}), pSiNP-H, pSiNP[TMZ], pSiNP-C$_{18}$, or pSiNP-C$_{18}$[TMZ] (equivalent to a dose of 3 mg kg^{-1} of TMZ) every other day for 10 days (n = 10). (B) Representative MRI images of U87MG tumor-bearing brain of mice after 5 rounds of drug administration. (C) Quantification of tumor volumes. Tumor volumes were calculated using Radiant DICOM viewer software. The data are presented as the mean ± standard error of the mean (SEM). A one-way ANOVA with Tukey's multiple-comparisons test was performed. **$p < 0.01$, ***$p < 0.001$, **$p < 0.01$, ***$p < 0.001$, and *n.s.* non-significant compared to the control; $^{\&\&}p < 0.01$ compared to TMZ. (D) Representative images of Ki67 and cleaved caspase-3 immunohistochemical staining in the tumor tissue of mouse brains. Photomicrographs were taken at 200× magnification. Scale bar, 200 μm. (E) Quantification of choromogenic areas in (D). The ratio of antigen-positive areas to the total area were calculated using Invitrogen™ Celleste™ Image Analysis Software (n = 4). A one-way ANOVA with Tukey's multiple-comparisons test was performed; *$p < 0.05$, ***$p < 0.001$ compared to control. (F) Kaplan–Meier survival plots of tumor-bearing mice in the different treatment arms. The study performed with six mice per treatment arm for statistical significance. A log-rank (Mantel–Cox) test was performed on the survival plot. *$p < 0.05$, **$p < 0.01$, ***$p < 0.001$ compared to the control; $^{\&}p < 0.05$ compared to the TMZ group.
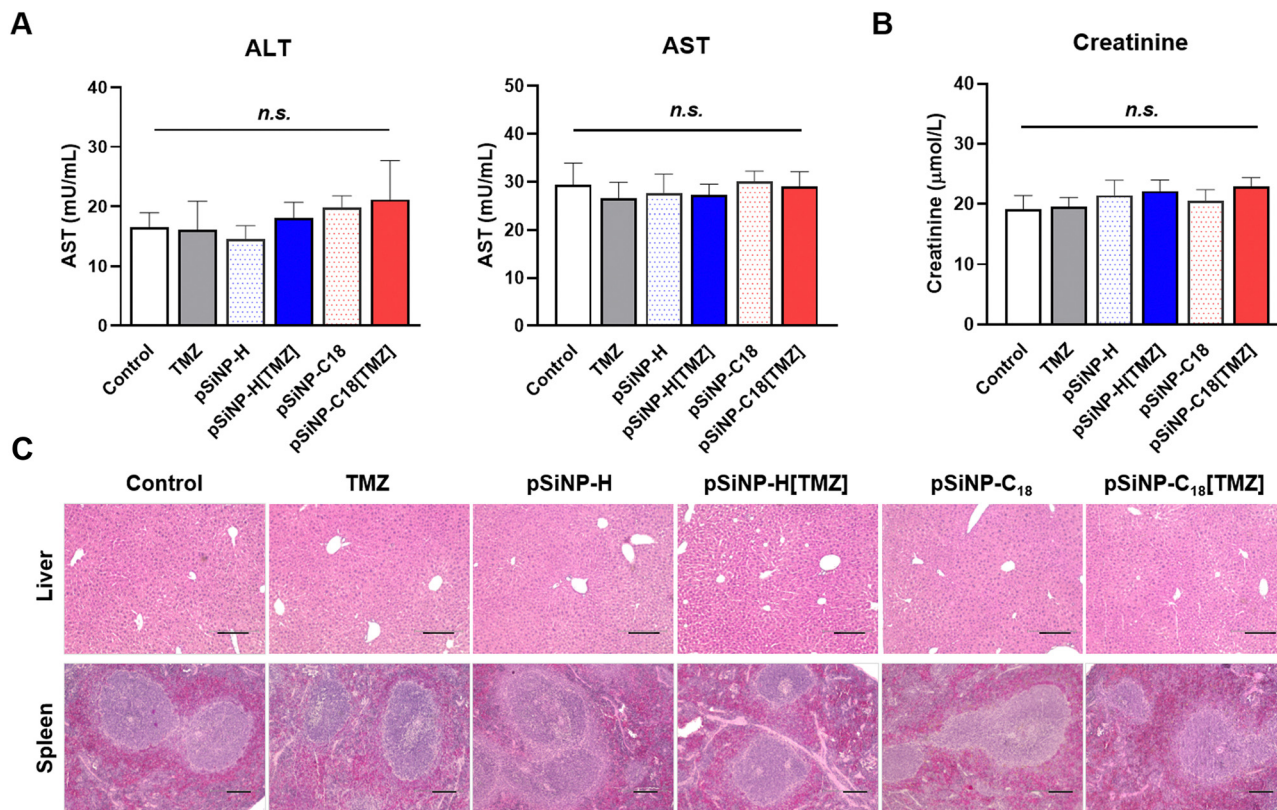
Fig. 5 Evaluation of *in vivo* toxicity of temozolomide (TMZ)-loaded porous silicon nanoparticles (pSiNPs). (A) ALT and AST levels in U87MG tumor-bearing mice following five administrations of the drugs ($n = 5–6$). The data are presented as the mean $\pm$ standard error of the mean (SEM). A one-way ANOVA with Tukey's multiple comparisons test was performed; *n.s.* denotes non-significant differences. (B) Creatinine levels in U87MG tumor-bearing mice following five administrations of the drugs ($n = 5–6$). The data are presented as the mean $\pm$ standard error of the mean (SEM). A one-way ANOVA with Tukey's multiple comparisons test was performed; *n.s.* denotes non-significant differences. (C) Representative images of hematoxylin- and eosin-stained liver and spleen sections. Photomicrographs were captured at $100\times$ magnification. Scale bar = 100 μm.

which were administered every other day for a total of five doses with resting periods of 10 days. The survival rates of the groups treated with TMZ, pSiNP-H[TMZ], and pSiNP-C$_{18}$[TMZ] were 33.3%, 66.7%, and 83.3%, respectively. Notably, pSiNP-C$_{18}$[TMZ] therapy significantly prolonged the survival of tumor-bearing mice compared with that of mice treated with either free TMZ or pSiNP-H[TMZ] over a period of 65 days (Fig. 4F). These findings collectively highlight the superior therapeutic efficacy of TMZ-loaded pSiNP-C$_{18}$.

Evaluation of the *in vivo* toxicity of TMZ-loaded pSiNPs

To assess the *in vivo* toxicity of the nanoformulations, we first measured the effects of the pSiNPs on plasma biochemical indices in mice subjected to five rounds of drug administration. Aspartate transaminase (AST) and alanine aminotransferase (ALT) are enzymes that are primarily located in the liver, and their elevated levels in the blood indicate liver cell injury. Plasma AST and ALT levels in the mice treated with TMZ-loaded pSiNPs or their vehicles showed no significant differences compared with those of the control group (Fig. 5A). Additionally, plasma creatinine levels were measured to evaluate kidney function. The mice treated with TMZ-loaded pSiNPs exhibited levels that were not significantly different from the

control group, demonstrating that neither pSiNP-H[TMZ] nor pSiNP-C$_{18}$[TMZ] exerts a toxic effect on kidney function (Fig. 5B). These findings were further supported by the absence of any pathological changes observed in the histological sections of the liver and spleen across all the mouse groups (Fig. 5C). In addition, treatment with TMZ-loaded pSiNPs or vehicles did not result in significant changes in the size of the inguinal lymph nodes (Fig. 5C). Taken together, these results suggest that pSiNPs exhibit no *in vivo* toxicity and demonstrate high biocompatibility within the tested dose range.

Conclusions

This study investigated the potential application of pSiNPs as a drug delivery vehicle to enhance the efficacy of TMZ for the treatment of GBM. Surface modification of pSiNPs with octadecane resulted in higher drug loading efficiency and a slower release profile than that observed with intact pSiNPs *in vitro*. These characteristics translated to greater peak concentrations of TMZ in the blood, thus facilitating the increased accumulation in the mice's brains. Taking advantage of the improved pharmacokinetic properties of TMZ-loaded octadecane-modified pSiNPs, their therapeutic use exhibited a superior anti-cancer effect in an intracranial GBM mouse model.

This journal is © The Royal Society of Chemistry 2024

J. Mater. Chem. B, 2024, **12**, 9335–9344 | 9343

TMZ-loaded octadecylated pSiNPs not only significantly reduced the brain tumor size but also significantly prolonged the survival of tumor-bearing mice without causing toxicity in healthy tissue. Taken together, this study demonstrates that the octadecane-modified pSiNPs are valuable tools for drug delivery to the central nervous system. Furthermore, TMZ-loaded octadecylated pSiNPs were identified as potential therapeutic agents for the treatment of central nervous system tumors.

Author contributions

Conceptualization: J. S. Kang, Y. Kim; investigation: S. Shin, H. Jo, T. Agura, S. Jeong, H. Ahn; formal analysis and data curation: S. Shin; writing – original draft: S. Shin; project administration: J. S. Kang, Y. Kim; funding acquisition: Y. Kim.

Data availability

The data supporting this article are provided as ESI† in a separate Excel file.

Conflicts of interest

There are no conflicts to declare.

Acknowledgements

References

1 R. Stupp, W. P. Mason, M. J. van den Bent, M. Weller, B. Fisher, M. J. B. Taphoorn, K. Belanger, A. A. Brandes, C. Marosi, U. Bogdahn, J. Curschmann, R. C. Janzer, S. K. Ludwin, T. Gorlia, A. Allgeier, D. Lacombe, J. G. Cairncross, E. Eisenhauer and R. O. Mirimanoff, *N. Engl. J. Med.*, 2005, **352**, 987–996.

2 F. Hanif, K. Muzaffar, K. Perveen, S. M. Malhi and U. Simjee Sh, *Asian Pac. J. Cancer Prev.*, 2017, **18**, 3–9.

3 S. Kumari, S. M. Ahsan, J. M. Kumar, A. K. Kondapi and N. M. Rao, *Sci. Rep.*, 2017, **7**, 6602.

4 Z. Song, X. Huang, J. Wang, F. Cai, P. Zhao and F. Yan, *Pharmaceutics*, 2021, **13**(8), 1270.

5 R. K. Oberoi, K. E. Parrish, T. T. Sio, R. K. Mittapalli, W. F. Elmquist and J. N. Sarkaria, *Neuro-Oncology*, 2016, **18**, 27–36.

6 T. I. Janjua, P. Rewatkar, A. Ahmed-Cox, I. Saeed, F. M. Mansfeld, R. Kulshreshtha, T. Kumeria, D. S. Ziegler, M. Kavallaris, R. Mazzieri and A. Popat, *Adv. Drug Delivery Rev.*, 2021, **171**, 108–138.

7 C. Lu, Y. Wei, X. Wang, Z. Zhang, J. Yin, W. Li, L. Chen, X. Lyu, Z. Shi, W. Yan and Y. You, *Mol. Cancer*, 2020, **19**, 28.

8 T. I. Janjua, Y. Cao, A. Ahmed-Cox, A. Raza, M. Moniruzzaman, D. T. Akhter, N. L. Fletcher, M. Kavallaris, K. J. Thurecht and A. Popat, *J. Controlled Release*, 2023, **357**, 161–174.

9 H. Strobel, T. Baisch, R. Fitzel, K. Schilberg, M. D. Siegelin, G. Karpel-Massler, K.-M. Debatin and M.-A. Westhoff, *Biomedicines*, 2019, **7**, 69.

10 J. Zhang, M. F. Stevens and T. D. Bradshaw, *Curr. Mol. Pharmacol.*, 2012, **5**, 102–114.

11 E. S. Newlands, M. F. G. Stevens, S. R. Wedge, R. T. Wheelhouse and C. Brock, *Cancer Treat. Rev.*, 1997, **23**, 35–61.

12 R. Jatyan, P. Singh, D. K. Sahel, Y. G. Karthik, A. Mittal and D. Chitkara, *J. Controlled Release*, 2022, **350**, 494–513.

13 K. Xu, L. Zhang, Y. Gu, H. Yang, B. Du, H. Liu and Y. Li, *Eur. Polym. J.*, 2021, **145**, 110232.

14 M. A. Westhoff, T. Baisch, V. J. Herbener, G. Karpel-Massler, K. M. Debatin and H. Strobel, *Biomedicines*, 2020, **8**, 151.

15 N. Singhal, S. Selva-Nayagam and M. P. Brown, *J. Neurooncol.*, 2007, **85**, 229–230.

16 G. Huang, N. Zhang, X. Bi and M. Dou, *Int. J. Pharm.*, 2008, **355**, 314–320.

17 P. Kumari, B. Ghosh and S. Biswas, *J. Drug Targeting*, 2016, **24**, 179–191.

18 J. Shen, W. Zhang, R. Qi, Z.-W. Mao and H. Shen, *Chem. Soc. Rev.*, 2018, **47**, 1969–1995.

19 U. Ikoba, H. Peng, H. Li, C. Miller, C. Yu and Q. Wang, *Nanoscale*, 2015, **7**, 4291–4305.

20 J. M.-P. Raul, M.-S. Miguel and T.-C. Vicente, *J. Nanophotonics*, 2010, **4**, 042502.

21 A. Bertucci, K.-H. Kim, J. Kang, J. M. Zuidema, S. H. Lee, E. J. Kwon, D. Kim, S. B. Howell, F. Ricci, E. Ruoslahti, H.-J. Jang and M. J. Sailor, *ACS Appl. Mater. Interfaces*, 2019, **11**, 23926–23937.

22 P. Granitzer and K. Rumpf, *Materials*, 2010, **3**, 943–998.

23 J.-H. Park, L. Gu, G. von Maltzahn, E. Ruoslahti, S. N. Bhatia and M. J. Sailor, *Nat. Mater.*, 2009, **8**, 331–336.

24 A. B. Foraker, R. J. Walczak, M. H. Cohen, T. A. Boiarski, C. F. Grove and P. W. Swaan, *Pharm. Res.*, 2003, **20**, 110–116.

25 J. Kang, J. Joo, E. J. Kwon, M. Skalak, S. Hussain, Z. G. She, E. Ruoslahti, S. N. Bhatia and M. J. Sailor, *Adv. Mater.*, 2016, **28**, 7962–7969.

26 J. M. Zuidema, T. Kumeria, D. Kim, J. Kang, J. Wang, G. Hollett, X. Zhang, D. S. Roberts, N. Chan, C. Dowling, E. Blanco-Suarez, N. J. Allen, M. H. Tuszynski and M. J. Sailor, *Adv. Mater.*, 2018, **30**, e1706785.

27 F. Wang, T. J. Barnes and C. A. Prestidge, *Pharmaceutics*, 2019, **11**(12), 634.

28 H. A. Santos, E. Mäkilä, A. J. Airaksinen, L. M. Bimbo and J. Hirvonen, *Nanomedicine*, 2014, **9**, 535–554.

29 J. F. Popplewell, S. J. King, J. P. Day, P. Ackrill, L. K. Fifield, R. G. Cresswell, M. L. di Tada and K. Liu, *J. Inorg. Biochem.*, 1998, **69**, 177–180.

30 S. Sheykhzadeh, M. Luo, B. Peng, J. White, Y. Abdalla, T. Tang, E. Mäkilä, N. H. Voelcker and W. Y. Tong, *Sci. Rep.*, 2020, **10**, 2320.

31 S. H. Lee, J. S. Kang and D. Kim, *Materials*, 2018, **11**, 2557.

9344 | *J. Mater. Chem. B*, 2024, **12**, 9335–9344

This journal is © The Royal Society of Chemistry 2024